

Transformation of Nanodiamonds to Onion-like Carbons by Ambient Electro spray Deposition

Deeksha Satyabola,[†] Tripti Ahuja,[†] Sandeep Bose, Biswajit Mondal, Pillalamarri Srikrishnarka, M. P. Kannan, B. K. Spoorthi, and Thalappil Pradeep*

Cite This: *J. Phys. Chem. C* 2021, 125, 10998–11006

Read Online

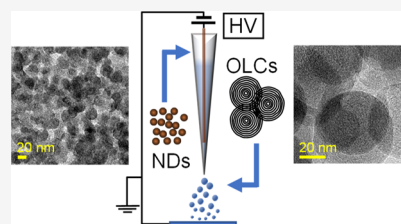
ACCESS |

Metrics & More

Article Recommendations

Supporting Information

ABSTRACT: Onion-like carbons (OLCs) are a class of fullerene-like circular nanoallotropes of carbon, typically synthesized from nanodiamond (ND) *via* thermal annealing, plasma spraying, and laser ablation. These methods require high temperature, high vacuum, or inert gas. Here, we report an ambient electro spray deposition (AESD) process to transform NDs (11 ± 1 nm in size) into OLCs (50 ± 13 nm in size) in water. Transmission electron microscopy (TEM), field emission scanning electron microscopy (FESEM), Raman spectroscopy, and X-ray photoelectron spectroscopy (XPS) were used for the characterization of NDs and OLCs. High-resolution TEM images showed an increased interplanar spacing from ND (0.23 nm) to OLC (0.39 nm). Raman spectra showed a shift in the ND peak from 1336 cm^{-1} to D-band at 1349 cm^{-1} , and XPS quantitatively estimated an increase in the graphitization ratio (sp^2/sp^3) from 0.95 to 3.16 after AESD. Comparison of electro spray with sonic spray confirmed that such a transformation required an external voltage as well. AESD was also performed for NDs dispersed in ethanol and acetonitrile, which showed a solvent-dependent transformation.



1. INTRODUCTION

Carbon has always amazed scientists with its unique ability to form bonds of various kinds, and this property is distinctly different from other elements in the periodic table.^{1,2} Due to this, several nanoallotropes of carbon have been identified since the discovery of fullerenes.^{3–6} These nanoallotropes can be converted to each other accompanied by a change in their hybridization.^{1,2} One such allotrope of carbon is nanodiamond (ND), also known as ultradispersed diamond (UDD). It has a core–shell-like architecture² with an sp^3 (diamond) core and sp^2 (graphitic) shells, surrounded by dangling bonds on the surface. NDs are transformed into sp^2 -hybridized carbon called onion-like carbons (OLCs) by the process of graphitization. OLCs are multilayered fullerene-like carbon shells, also called carbon nano-onions (CNOs), or carbon onions (COs).^{7,8} They have demonstrated their applicability in electrical double-layer capacitors⁹ and high-performance supercapacitor electrodes¹⁰ for energy storage due to high charge–discharge rates⁹ and possess capacitance similar to carbon nanotubes. High conductivity and compatibility to form composites with other inorganic materials have made them ideal candidates for solar cell applications.¹¹ They have also been studied for biomedical imaging,¹² biochemical sensing,¹³ and therapeutic nano-carriers¹⁴ due to nontoxicity, suitability, and covalent functionalization with most naturally occurring biomolecules. Nitrogen-doped CNOs with gold¹⁵ and copper¹⁶ nanoparticles have enabled the formation of nanocomposite electrochemical sensors and efficient oxygen reduction electrocatalysts,

respectively. COs have also been utilized for water treatment¹⁷ because of their ability to absorb heavy metal ions.

Besides the applications of OLCs in capacitors, sensors, water treatment, and so forth, there have also been efforts to discover new methods for the synthesis of OLCs. The OLCs were synthesized initially using carbonaceous materials or amorphous carbon soot *via* heat treatment above 2500 K¹⁸ and high-energy electron beam irradiation.¹⁹ Both the precursors and methods used for the synthesis of OLCs have been modified over time.^{20–28} ND, methane, propane, and aromatic compounds have been utilized to obtain various structures of OLCs ranging from spherical and polyhedral to hollow or those containing metal cores, through annealing,^{20,21} chemical vapor deposition (CVD),²² carbon ion implantation,²³ arc-discharge,²⁴ pyrolysis,^{25,26} and so forth. Among all these methods and precursors, large quantities of OLCs have been synthesized from ND due to the ease of synthesis and availability.⁷ The annealing of ND to OLCs introduced by Kuznetsov *et al.* requires a high temperature of 1273–1773 K and high vacuum.²⁰ Later, Gubarevich *et al.* introduced a plasma-spray method for the synthesis of OLCs from NDs, which required a current of 100 kA and arc discharge at ~ 10

Received: January 8, 2021

Revised: April 27, 2021

Published: May 13, 2021



kPa of argon.²⁷ The conversion of ND to a new diamond, through CO as the intermediate, accompanied by a high-temperature laser-induced transformation has also been reported.²⁸

In this paper, we have introduced a simple technique called ambient electro spray deposition (AESD) for the transformation of ND to OLC at room temperature and atmospheric pressure. AESD is a subset of electro spray ionization (ESI) that has immense applications in mass spectrometry (MS).²⁹ AESD has been proved to be a promising technique for the synthesis of functional nanomaterials as well.^{30–32} Li *et al.* have used ESI for the synthesis of silver and gold nanoparticles³⁰ and showed an improved catalytic activity by their use in the reduction of *p*-nitrophenol. Our group has also reported the formation of metallic nanobrushes of silver³¹ and distinct phases of Cu₂S³² using AESD.

Our method of transformation of ND to OLC involves two steps: (1) ES of ND suspension and (2) soft-landing/deposition of the product on a conducting surface. ND before ES and the transformed product (OLC) after ES were thoroughly characterized by transmission electron microscopy (TEM), field emission scanning electron microscopy (FESEM), Raman spectroscopy, and X-ray photoelectron spectroscopy (XPS). To understand the mechanism of transformation of NDs to OLCs, a comparative study of ES and sonic spray (SS) was performed. While SS leads to graphitization of ND as in ES, the final nanoallotrope obtained using SS differed from OLCs. This proved that an external voltage is necessary and is essential to produce OLCs at ambient temperature and atmospheric pressure. Additional parameters that distinguish ES from SS such as the presence of charge and electric field at the spray tip and Laplace pressure on the droplet were also evaluated. Furthermore, we changed the solvent from water to acetonitrile (MeCN) and ethanol (EtOH) to understand the effect of the solvent on graphitization. Transformation of ND to OLCs was facile in water as compared to MeCN and EtOH. Factors such as dielectric constant and surface tension vary in different solvents, which affect ES and play a significant role in the transformation.^{33–36} Additionally, understanding the interactions between ND and solvent molecules is also required. Such an interaction has been studied in detail by Holt *et al.*³⁷ between ND and EtOH vapors. They have mentioned a possibility of hydrogen bonding between the polar functionalities on ND and EtOH molecules, which may stabilize the surface of ND. Other attempts to understand the interaction and solubility of ND are also known by dissolving it in various polar and nonpolar solvents.³⁸ All of them are known to stabilize the ND particles and form dispersions, ascertaining that the interactions between adjacent ND particles³⁹ and with the solvent³⁸ molecules are pertinent to understand the transformation.

2. MATERIALS AND EXPERIMENTAL METHODS

2.1. Materials. ND powder, $\geq 97\%$ purity, was purchased from Sigma-Aldrich. Borosilicate glass capillaries (outer and inner diameters of 1.5 and 0.86 mm, respectively) were prepared with a tip diameter of 30–45 μm (determined using an optical microscope) to form a nanospray emitter using a micropipette puller (P-97), Sutter instrument, USA. Indium tin oxide (ITO) glass slides were purchased from Zhuhai Kaivo Electronic Optoelectronics Technology Co., Ltd. Other

reagents such as MeCN and EtOH were of analytical grade and used without further purification. Deionized (DI) water ($\sim 18.2 \text{ M}\Omega$) obtained from Milli-Q was used throughout the experiments.

2.2. Preparation of ND Suspension and Substrates for Characterization. ND (1.5 mg) was dissolved in DI water (1 mL) to obtain a 125 mM stock suspension. Concentration was evaluated in terms of the C content present. It was mixed thoroughly on a SPINIX vortex shaker for 3 min and successively diluted to prepare a 1.25 mM ND suspension. The diluted suspension (1.25 mM) of ND was used for ES and SS because low concentrations are most suitable in nanoESI.³⁶ Similarly, ND suspension (1.25 mM) was prepared in MeCN and EtOH to examine the effect of solvents on the transformation of ND. The suspension was electro sprayed on the carbon-coated copper grid by placing it on top of an ITO glass slide (22 mm \times 22 mm \times 1.1 mm) for HRTEM analysis. The same copper grid was fixed on a conducting carbon tape and used for FESEM analysis. The electro sprayed ITO glass slide was used directly for Raman and XPS characterization.

2.3. Instrumentation. TEM and HRTEM measurements of ND, before and after ES, were performed using a JEOL3010 at an accelerating voltage of 200 kV. FESEM measurements were performed using a Thermo scientific Verios G4 UC having a retractable detector. Confocal Raman imaging of ND, before and after ES, was performed on a WITec alpha300 S with a frequency-doubled Nd:YAG laser at 532 nm with 10 mW laser power, 2 s acquisition time, and 20 accumulations. To identify the chemical oxidation states and for quantitative estimation of ND and OLC, XPS was performed with an electron spectroscopy for chemical analysis (ESCA) probe temperature-programmed desorption (TPD) spectrometer of Omicron Nanotechnology with a polychromatic Al K α ($h\nu = 1486.6 \text{ eV}$) source having a step size of 0.08 eV. The binding energies (BEs) of all the elements were calibrated with respect to C 1s at 284.8 eV. The percentage of peak area was calculated by taking the relative sensitivity factor (RSF) of carbon as unity.

2.4. Ambient Electro spray Deposition (AESD) Setup. The AESD setup (Figure 1) used for ES was composed of an

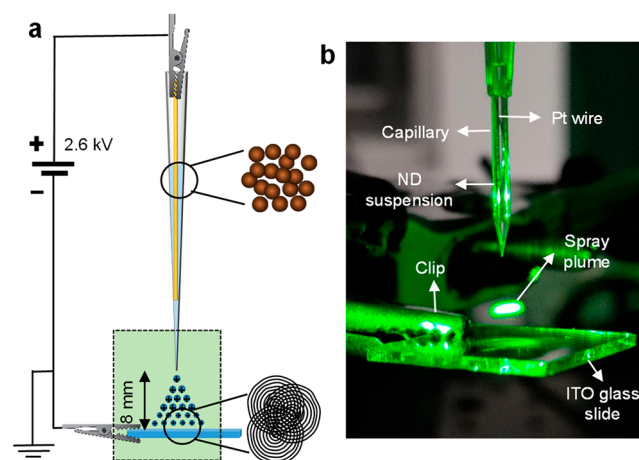


Figure 1. (a) Schematic representation of the AESD setup. (b) Magnified optical image of the rectangular area in (a) shows the spray plume soft-landing on the ITO glass slide. The spray plume in (b) was visualized with a laser.

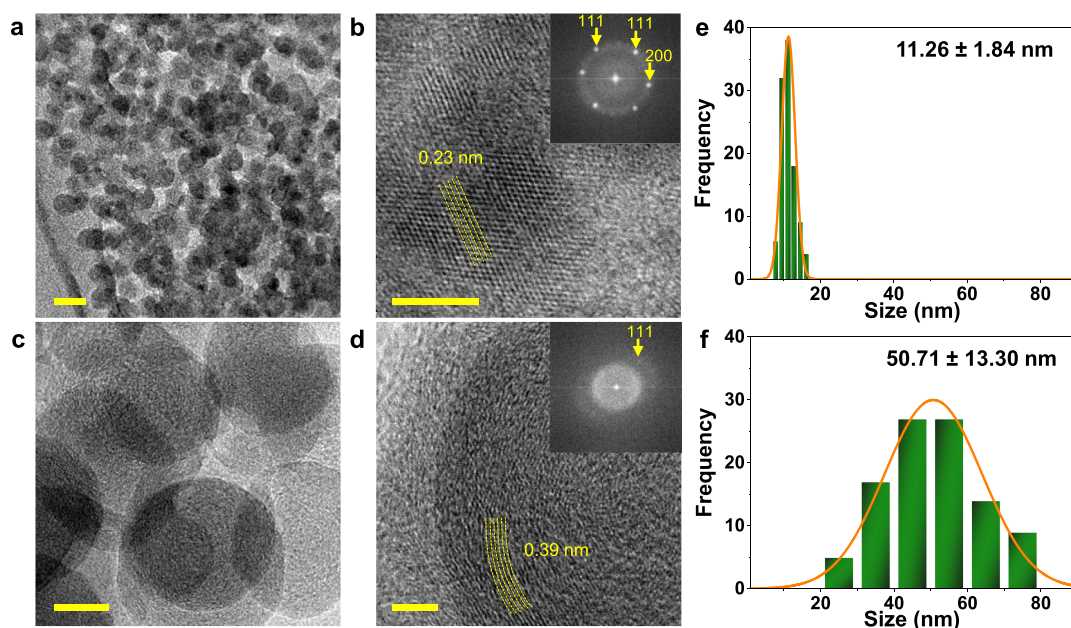


Figure 2. TEM and HRTEM images of NDs (a,b) depicting a lattice spacing of 0.23 nm, and OLCs (c,d) obtained after ES with a lattice spacing of 0.39 nm. Insets of (b,d) show the corresponding FFT images. Particle size distribution gives a mean size of (e) 11.26 ± 1.84 nm for ND and (f) 50.71 ± 13.30 nm for OLC. The scale bars in (a,c) are 20 nm and (b,d) are 5 nm.

external voltage source supplied by a variable DC power supply and a nanospray assembly. The nanospray assembly was made of a nanoESI capillary, platinum (Pt) wire (0.2 mm in diameter), and ITO glass slide. The Pt wire was inserted in a borosilicate capillary already filled with the ND suspension using a microinjector pipette tip. The distance between the capillary tip to the ITO glass slide was 8 mm. The assembly was supported by a clamp and stand to keep it stable and firm. The positive terminal of the voltage source was connected to the Pt wire, and the negative terminal was connected to the ITO glass slide, which was grounded. It was found that ES was possible only in the positive mode. Therefore, the same was followed throughout all the experiments. The applied voltage and time required to collect 20 μL of the sample in the spray plume were 2.6 kV and 1 h, respectively. The potential and tip to capillary distance were optimized as described by Jana *et al.*³²

2.5. Sonic Spray (SS) Setup. The SS setup (Figure S5) was composed of a N_2 gas cylinder connected sideways to a T-connector, a fused silica capillary (inner and outer diameters were 150 and 300 μm , respectively) connected from the top of the T-connector, and a vial (1.5 mL) that collects the SS. ND suspension (1.25 mM) was loaded in a 500 μL Hamilton syringe connected with the silica capillary using a union connector and placed on the syringe pump. The syringe pump continuously infused the ND suspension at a constant flow rate of 5 $\mu\text{L min}^{-1}$, which generated uncharged microdroplets on contact with high-pressure N_2 . These microdroplets were collected for 3 h in the vial and later diluted with 50 μL of DI water for TEM and Raman. Subsequently, the SS was performed at different pressures (5, 10, and 15 psi) to optimize the pressure-induced graphitization.

3. RESULTS AND DISCUSSION

3.1. Transformation of NDs to OLCs Using AESD. In AESD, a nanoESI capillary containing ND suspension (1.25 mM) was connected to the positive terminal of an external

voltage source (2.6 kV) (Figure 1a). As a result, a positive charge was accumulated on the ES plume of ND, which was soft-landed on a negatively charged counterelectrode, an ITO glass slide. This region is marked by a rectangle in Figure 1a. This is shown as an optical image in Figure 1b.

3.2. Characterization of ND before and after ES. TEM images of NDs before and after ES are shown in Figure 2a–d. The ND particles are spherical and highly aggregated (Figure 2a). The aggregation of NDs was attributed to the Coulombic interaction among the surface functionalities of adjacent particles.³⁹ NDs showed the characteristic diamond lattice (Figure 2b) with a lattice spacing of 0.23 nm due to the (111) plane, comparable to that of diamond (0.21 nm). The product of ES shown in Figure 2c,d was characterized as unique onion-like concentric circular structures called OLCs. Unlike ND, the OLCs are large and composed of concentric circular rings. The increase in the size of OLCs is evident by the respective particle size distribution of ND and OLCs shown in Figure 2e,f. The average particle size of ND was 11.26 ± 1.84 nm, which increased to 50.71 ± 13.30 nm in OLCs (Figure 2e,f). The HRTEM image of OLCs (Figure 2d) showed a lattice spacing of 0.39 nm. This lattice spacing of OLCs varied from 0.33 to 0.35 nm.^{20,27,28} Such a variation is attributed to the different synthetic protocols followed for this work compared to the other conventional routes. The majority of OLCs obtained by ES are overlapped with others or are deformed slightly along the periphery on account of their soft-landing process on the ITO surface (Figure 2c). It was difficult to discern individual rings inside the OLCs most of the time; however, the concentric circular nature was noticeable in the HRTEM image (Figure 2d). The FFT images of NDs and OLCs are shown as insets in Figure 2b,d, indicating the prominent planes in each. The FFT of ND shows three pairs of bright spots indicating its crystalline nature, and OLCs show a concentric ring pattern that represents the multilayered fullerene-like carbon shells as described by Isabel *et al.*⁴⁰ Moreover, some of the FFT images of OLCs had two intense

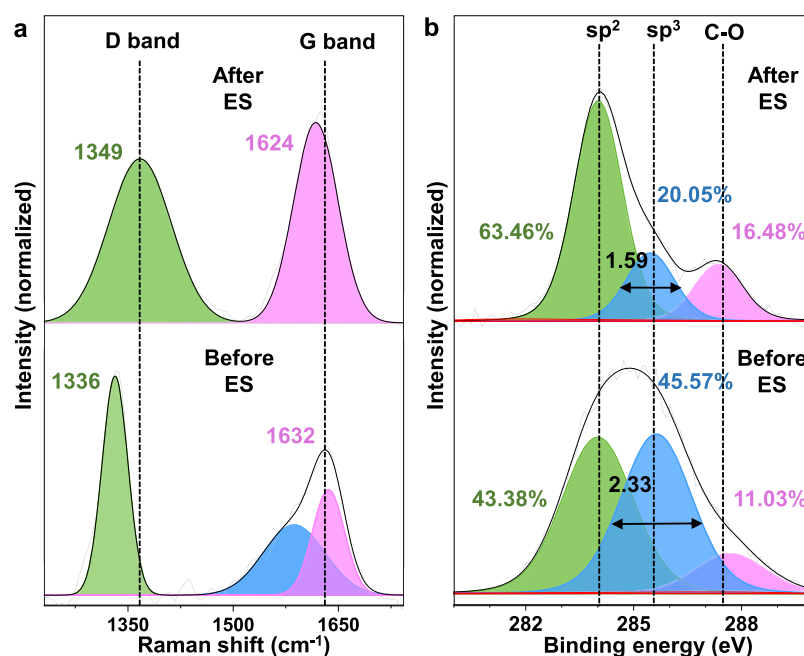


Figure 3. Stacked Raman spectra (a) showcasing shift in the ND peak at 1336 cm⁻¹ (before ES) to a broad D-band (green) at 1349 cm⁻¹ (after ES), graphitic sp²-C peak at 1632 cm⁻¹ also got shifted to the G-band (pink) at 1624 cm⁻¹. Stacked C 1s core-level XPS spectra (b) of drop-casted ND (before ES) and OLCs (after ES) provide the percentages of sp²-C (green), sp³-C (blue), and C–O bound C (pink). The as-obtained and fitted spectra are represented by gray and black curves, respectively.

spots (not shown here), which correspond to parallel layers characteristic of graphitic structures. Such a discrepancy was attributed to the presence of sp²-graphitic cover over ND. This was because the spray conditions were not adequate to convert all NDs into OLCs.

The transformation of ND to OLC took place over a considerable region. It is evident by the large-area TEM images of ND and OLC shown in Figure S1a,b.

We chose FESEM to see the morphological variations in ND before and after ES. The distinct morphology and surface structure of ND and OLCs were difficult to perceive; nonetheless, the transformation from highly agglomerated ND particles (Figure S2a) to overlapping OLCs (Figure S2b) was seemingly evident. OLCs were observed distinctly due to their large size in contrast to ND particles; the average size of OLCs was 33–46 nm (Figure S2b).

The applicability of AESD to form OLCs at higher concentrations (5 mM of ND suspension) was also tested. Figure S3a–d shows the TEM and FESEM images of the product obtained upon ES of 5 mM aqueous suspension of ND, which also resembled OLCs. Close inspection of the TEM images revealed the concentric nature of the OLCs, similar to other concentrations (Figure S3a,b). The size of OLCs varied in a wide range from 31 to 50 nm as evident by the FESEM images (Figure S3c,d).

Besides monitoring the effect of concentration on the transformation, it is equally important to know the formation of the same product on different substrates after ES. To show that ES on the ITO glass slide and carbon-coated copper grid resulted in the same product, the deposited product on the ITO glass slide was removed by scratching; then, the resulting product was dissolved in 50 μL of DI water and drop-casted on a TEM grid. Respective TEM and HRTEM images of the product obtained upon direct ES on an ITO glass slide are shown in Figure S4a,b, respectively. These images also showed

the formation of concentric circular rings, but they were slightly distorted which may be due to the scratching of the thin-layered product from the ITO surface. Thus, the transformation was substrate-independent, to a significant extent.

XRD measurements of ND and OLC are important for easy visualization of the change in the lattice structure of ND upon transformation to OLC. The OLCs were deposited as a thin film after ES on the ITO glass slide, and the signals obtained were weak with intense background due to ITO. Therefore, we moved to alternative techniques such as Raman spectroscopy and XPS.

ND is a suitable Raman analyte that possesses distinct vibrational features. However, its photoluminescence nature creates a huge rise in the background of the Raman spectrum. The background associated with the vibrational features of ND can be reduced by decreasing the wavelength of the excitation laser employed because the lower wavelength such as 230 nm matches with the band gap (5.4 eV) of ND.⁴¹ As the excitation laser (532 nm) has a wavelength higher than 230 nm, the background in the Raman spectrum was corrected using suitable baseline correction. The spectra were normalized, and peaks were fitted thereafter. Figure 3a shows the stacked Raman spectra of ND before and after ES. In Raman spectra, peak position and full width at half-maximum (fwhm) (Figure 3a) provide useful information pertaining to the change in the hybridization of ND (sp³) to OLCs (sp²). Before ES, ND shows an intense and sharp peak at 1336 cm⁻¹ with 43 cm⁻¹ fwhm value due to the presence of a cubic lattice of sp³-diamond in the ND core. It also showed a broad peak in the region of 1580–1650 cm⁻¹, which was fitted with a combination of two peaks (103 and 54 cm⁻¹ fwhm) and corresponds to the G-band of the graphitic shell surrounding the ND core, specifically the in-plane stretching vibration of the sp² C–C bonds. The broadness of the G-band is also

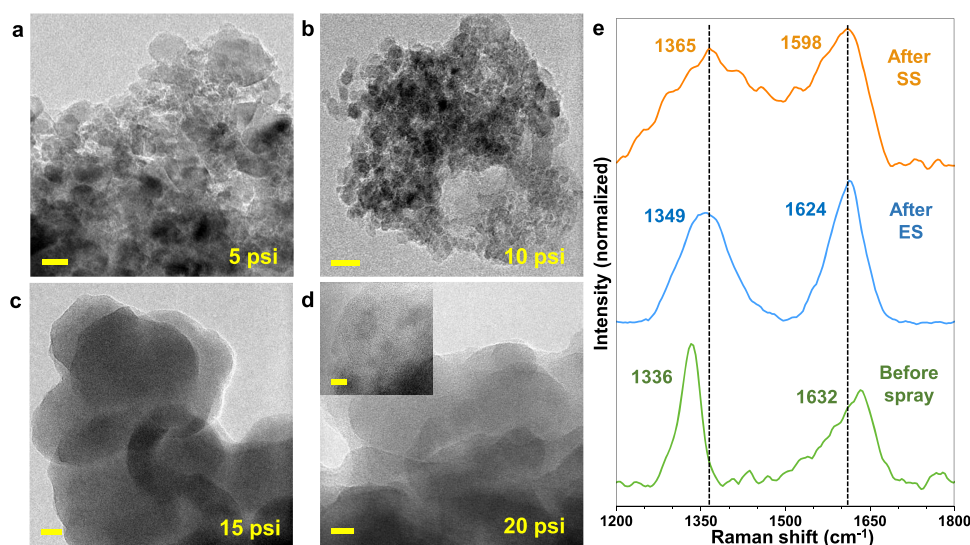


Figure 4. TEM images (a–d) of the product obtained after SS at 5, 10, 15, and 20 psi. The inset of (d) shows its HRTEM image. Comparative Raman spectra (e) showing shifts in the peak positions before spray (green), after ES at 2.6 kV (blue), and after SS at 20 psi (orange). The scale bar in (a–d) is 20 nm each [inset of (d) is 5 nm].

attributed to the presence of several other functionalities⁴² on the surface, such as $\nu(\text{C}=\text{C})$, $\delta(\text{O}-\text{H})$, mixed sp^2 – sp^3 carbon, and some defects appearing on its surface. After ES, the sharp ND peak at 1336 cm^{-1} (43 cm^{-1} fwhm) is blue-shifted to a broader peak at 1349 cm^{-1} (105 cm^{-1} fwhm). The latter was assigned to the D-band of disordered sp^2 -C over ND. Another sp^2 -C peak appears at 1632 cm^{-1} (before ES), which was fitted with two peaks at 1586 cm^{-1} (103 cm^{-1} fwhm) and 1636 cm^{-1} (54 cm^{-1} fwhm), showed a red shift to a relatively sharp and single G-band around 1624 cm^{-1} (75 cm^{-1} fwhm) after ES, corroborated with the literature.^{42–44} In conventional annealing methods, fwhm values of the diamond feature and that of the G-band increase up to $600\text{ }^\circ\text{C}$ and decrease subsequently with a further increase in temperature.⁴³ In ES, the fwhm of the diamond peak increased and that of the G-band decreased after ES. Compared to detonated ($\sim 40\text{ cm}^{-1}$) or annealed ND, electrosprayed ND (105 cm^{-1}) showed a large increase in fwhm. The physical reason behind the variation of fwhm values in detonation and annealed ND is due to the phonon confinement effect as explained by Mermoux *et al.*⁴² The detailed reason behind the large increase in fwhm after ES is yet to be understood. A table showing a comparison of observed Raman peaks with the authentic OLCs from the literature⁷ is mentioned in Supporting Information, Table S1.

It was difficult to convert all the ND suspension into OLCs because the spray conditions governed the overall transformation. Therefore, a better approach to estimate the amount of ND transformed to OLC was using XPS. It can evaluate the amount of OLCs formed based on the percentage of C transformed from sp^3 to sp^2 . Quantification of sp^2 -C was achieved by performing high-resolution XPS of ND before and after ES. High-resolution spectra were fitted using Shirley background with an equal fwhm for all peaks. Figure 3b shows the C 1s core-level XPS spectra of the NDs (before ES) and OLCs (after ES). The sp^2 - and sp^3 -hybridized C appear at binding energies of 284 and 285.5 eV, respectively. The surface of ND also contains oxygen-bound functionalities that are represented by the C–O peak at 287.5 eV. The fwhm of the C 1s peak was 2.33 eV in ND and 1.59 eV in OLC. The peaks were in good agreement with the existing literature and

showed a decrease in the fwhm values from ND to OLC, and such a difference is attributed to intrinsic charge discrepancy.⁴⁵ The area under each deconvoluted C1s peaks yields the percentage of sp^2 -C, sp^3 -C, and C–O. In the transformation of NDs to OLCs, the proportion of sp^2 -C has increased by 20% with a simultaneous decrease in sp^3 -C. The sp^2/sp^3 ratio has increased from 0.95 in ND to 3.16 in OLCs (calculation S1, sp^2/sp^3 ratio), confirming the formation of OLCs.

3.3. Comparison between ES and SS of ND. To understand the mechanism and the parameters essential for the transformation, we performed an SS experiment, which was devoid of an external voltage. The schematic of the sonic spray setup is shown in Figure S5. A Hamilton syringe containing ND suspension (1.25 mM) was discharged *via* a silica capillary at a flow rate of $5\text{ }\mu\text{L min}^{-1}$ using a syringe pump. N_2 gas was maintained at 20 psi, which generated microdroplets of ND suspension, a phenomenon similar⁴⁶ to that of ES.

Figure 4a–d shows the TEM images of the product of SS obtained at varied pressures from 5 to 20 psi. Fine aerosol droplets were obtained in the spray in this range. Most of the ND particles remain unmodified at 5 and 10 psi (Figure 4a,b), but with an increase in pressure to 15 and 20 psi (Figure 4c,d), transformation resulted in mild graphitization in ND. The nanostructures obtained using SS were different in morphology from the OLCs obtained by ES. The structure, shape, and size of the product of SS were highly distorted and imperfect, compared to the symmetrical and circular OLCs obtained through ES.

To confirm the graphitization in SS, Raman spectral analysis was performed. Figure 4e shows stacked Raman spectra of ND, before spray, after ES, and after SS. The ND peak before spray at 1336 cm^{-1} was broadened and shifted to 1365 cm^{-1} upon SS by 29 cm^{-1} , compared to a shift of 16 cm^{-1} on ES. This shift was attributed to the D-band of graphite in both ES and SS. Similarly, the peak at 1632 cm^{-1} was blue-shifted to 1598 cm^{-1} , which corresponds to the G-band of C after SS. The fwhm of the diamond peak in SS also increased to 184.94 cm^{-1} , compared to 105.05 cm^{-1} in ES. These shifts confirmed the pressure-induced graphitization of ND in the SS. This comparison revealed that high pressure facilitates the process

of graphitization. However, SS could not produce the OLCs of defined shape and morphology as obtained *via* AESD.

AESD and SS also differ in terms of the radius of the capillary tip used, which is crucial to consider as it decides the size of the droplet. The droplet size is smaller in AESD that employs the nano-ESI mechanism than SS that is based on ES, which may favor the transformation to OLCs in the former. To check that we electrospayed the ND suspension with a fused-silica capillary (tip radius: 75 μm , three times larger than the borosilicate capillary used in nano-ESI). It was observed that concentric OLCs were formed, but most of them had irregular shapes which were fused to each other along the edges compared to separate OLCs produced using AESD (Figure S6). Thus, the transformation was weakly dependent on the droplet size. Therefore, we concluded that an SS experiment with voltage can also form OLCs.

It is difficult to study the mechanism of the transformation of the sp^3 -hybridized diamond core in ND to sp^2 -hybridized OLC, due to the inherently small size and high speed of the microdroplets formed during ES, which demands sophisticated high-speed cameras coupled with microscopy to capture the ultrafast plume in ES.⁴⁷ A comparison of ES with SS aided in accounting for the external factors responsible for the transformation of NDs to OLCs *via* AESD. The optimized parameters used in ES and SS are listed in Table 1.

Table 1. Parameters Used in ES and SS

parameter	ES	SS
voltage applied (kV)	2.6	N/A
charge on the droplet ²⁹ (C)	$\sim 10^{-14}$	N/A
electric field (V m^{-1})	1.45×10^7	N/A
radius of the capillary tip (μm)	25	75
Laplace pressure (kPa)	5.8	2

Considering the importance of these parameters at 2.6 kV, the electric field³³ at the tip of the capillary was calculated as $1.45 \times 10^7 \text{ V m}^{-1}$ (calculation S2a, electric field at the capillary tip). Such a high electric field at the capillary tip is responsible for the generation of droplets by ES, with a charge²⁹ of $\sim 10^{-14}$ C. Furthermore, the droplet present on the curved surface of the capillary tip possesses an interfacial tension, which can be related to the pressure inside the droplets and radius of curvature of the capillary used. This pressure is termed as Laplace pressure and can be calculated at the capillary tip interface for ES and SS, using the relation mentioned by Lee *et al.*⁴⁸ (calculation S2b, Laplace pressure at the capillary tip). The Laplace pressure in the capillary was higher in ES compared to SS by 3.8 kPa, attributed to the smaller radius of curvature of the capillary used in ES. An increase of 3.8 kPa in ES was insignificant for rupturing the ND lattice. Thus, additional parameters such as the electric field also should play an important role. ES uses external voltage, which generates a high electric field, and charge on the droplet, unlike SS. This reaffirmed that the transformation to OLCs is highly dependent on the presence of charge and high electric field on the droplet at the capillary tip.

Besides the role of the Laplace pressure and electric field, several rearrangements in the bond can happen as the droplet is discharged from the capillary tip. The process of spray takes microseconds. Various other phase transformations are known^{49–51} to happen at ultrafast and femtosecond time scales such as the nonthermal melting in Ge semiconductors,⁴⁹

superheating, and melting of bulk ice.⁵¹ Since these phase transformations involve rearrangements in bonds; we suggest that the transformation of ND to OLC is facile on a short-time scale. However, the actual mechanism of such a transformation is still elusive. We may conclude that high Laplace pressure combined with the electric field and charge on the droplets facilitates the conversion in ES.

3.4. Effect of Solvents on the Formation of OLCs *via* AESD. ES is highly dependent on the physical and chemical properties of the solvent such as polarity, dielectric constant (ϵ), and surface tension (γ).^{29,36} To understand the effect of these properties of the solvent on the conversion of ND to OLCs, we performed the ES in MeCN and EtOH in addition to DI water. The parameters of ES, namely, capillary-tip to ITO distance, the concentration of ND suspension, and duration of spray, were kept constant throughout the ES performed with various solvents. MeCN and EtOH showed a liquid jet spray at 2.6 kV due to which the external voltage was reduced to 1.4 kV to get a proper spray plume. This is because MeCN and EtOH have low surface tension, which allowed the formation of a Taylor cone at a lower voltage compared to DI water.³⁴ The properties which affect the ES in solvents are presented in Table 2.

Table 2. Factors Affecting ES in DI Water, MeCN, and EtOH

solvent	polarity	ϵ (F/m)	γ (dyne/cm)	V (kV)	conversion
DI water	1	78.54	72.00	2.6	high
MeCN	0.46	36.64	28.40	1.4	low
EtOH	0.65	24.60	22.10	1.4	low

The transformation was found to be most favorable with DI water in the regime of parameters used. The high dielectric constant and polarity of water are known to stabilize the high charge states and multiply charged species more efficiently.²⁹ On the other hand, high surface tension of water makes it difficult to release the spray in the form of a stable, gentle spray plume at a lower voltage.³⁴ Since external voltage is an important criterion for the formation of OLCs as inferred by the comparison of ES and SS, a high voltage must have facilitated the conversion to OLCs better in water compared to MeCN and EtOH. Thus, the overall effect led to the transformation of ND particles in DI water more efficiently than in the other two solvents.

Figure 5a,b shows the TEM images of ND before and after ES, respectively, in MeCN. Similar to DI water, the extremely aggregated nature of ND particles was retained in MeCN. The average size of ND particles in MeCN also stayed the same, which is apparent from Figure 5a. After ES, mild graphitization was seen, but no OLCs were observed (Figure 5b) and large amounts of ND particles stayed unmodified. Corresponding Raman spectra corroborated the TEM results (Figure 5e). The sharp peak at 1335 cm^{-1} before ES in MeCN was shifted slightly to a higher wavenumber at 1339 cm^{-1} after ES. As the change was within the instrumental resolution (4 cm^{-1}), it was concluded that the ND was affected negligibly after ES in MeCN. The G-band of ND in MeCN at 1642 cm^{-1} on the other hand was slightly red-shifted at 1639 cm^{-1} after ES, but it lies in the same $1580\text{--}1650 \text{ cm}^{-1}$ region.

Figure 5c,d shows the TEM images of ND dissolved in EtOH before and after ES. In this case also, graphitization was observed after ES (Figure 5d), but most of the ND particles

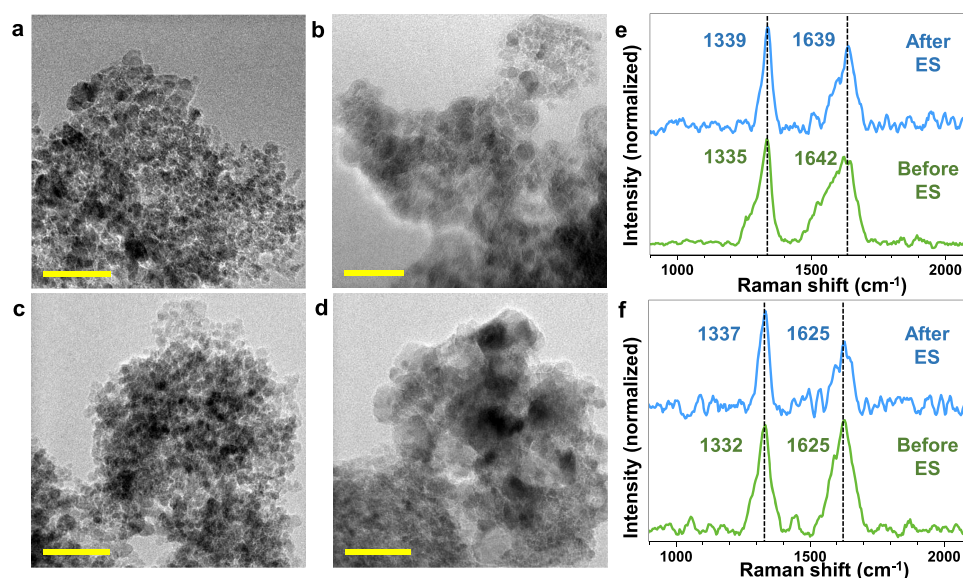


Figure 5. TEM images of ND dissolved in MeCN (a,b) and EtOH (c,d) before and after ES, respectively. Stacked Raman spectra of ND dissolved in MeCN (e) and EtOH (f) before (green) and after (blue) ES. The scale bars in (a–d) are 50 nm.

remain untransformed. Raman spectra of ND in EtOH before and after ES are shown in Figure 5f. The ND sp^3 -C peak at 1332 cm^{-1} before ES got shifted to 1337 cm^{-1} , whereas the broad G-band at 1625 cm^{-1} stayed at the same position after ES. As mentioned earlier, the G-band is a contribution of several functionalities present on the ND surface. A major contribution to the G-band can arise due to hydrogen bonding of the polar surface functionalities on the ND surface with solvent molecules, due to which the Raman spectra of ND in MeCN and EtOH are significantly different.

The transformation of ND to OLCs in ES involves a complex mechanism as evident by the large increase in the size of OLCs in comparison to NDs. Such a complex mechanism may include transport reactions, which are stated as reactions in which a substance goes to a vapor state and comes back to the parent state in a pure form.⁵² ND suspension can undergo a similar process by application of external voltage during AESD, which evaporates some of its particles to a gaseous state that can settle on the surface as OLCs. Although an in-depth computational study may reveal the exact mechanism behind the transformation, so far, a complete understanding of the mechanism is elusive.

We propose that the reaction mechanism for graphitization from sp^3 -hybridized C can be triggered on the surface and proceed inward, resulting in OLCs. Understanding the interaction of ND with charged solvent species at the nanoscale can be a vital step in determining the pathway of transformation in ES. For instance, in the case of water as a solvent, it is possible that the positively charged suspension in the nanoESI capillary can provide an impetus for protonation of the surface functionalities, followed by their elimination.⁵³ This leads to the formation of a positive charge on the surface of ND. To compensate for the positive charge on the surface of ND, either a rearrangement or $C=C$ bond formation from the neighboring carbon atoms may take place. A similar process happens at other locations on the surface of ND, which triggers graphitization on the surface, and this may proceed inward. A series of such events could lead to OLC formation.

4. CONCLUSIONS

In conclusion, we devised a methodology for the transformation of NDs to OLCs using AESD. TEM, FESEM, Raman, and XPS were used to characterize NDs and the ES-produced material. An increase in size and lattice spacing was observed in the TEM and HRTEM micrographs. Raman and XPS spectra showed the conversion of sp^3 - to sp^2 -hybridized carbon. The characteristic vibrational peak of the sp^3 core in ND was shifted from 1336 to the D-band at 1349 cm^{-1} with a decrease in intensity in the Raman spectra which showed that the transformation to OLCs occurred after ES. Although a complete mechanism behind the transformation of NDs to OLCs during AESD is difficult to comprehend at this stage, a comparison between ES and SS confirmed that high voltage is an essential condition for the generation of charged microdroplets to form OLCs. The application of high-pressure gas on SS led to graphitization; however, OLCs were not obtained. In addition, due to the dependency of ES on the type of solvent used, AESD was performed in three solvents, namely, DI water, MeCN, and EtOH. The high polarity and dielectric constant of DI water tend to easily stabilize various charged species formed during ES, but its high surface tension compared to the other two made the formation of the Taylor cone difficult. Consequently, the transformation of ND in DI water occurred more efficiently than MeCN and EtOH. In this way, AESD in its simple form has served as an efficient technique for the transformation of NDs to OLCs under ambient conditions, compared to the conventional methods that require high temperature and pressure. The current sp^2/sp^3 conversion ratio of NDs to OLCs (0.95 – 3.16) can be scaled up using a multispray technique. AESD also avoids the use of subsidiary gas spray such as ESI and can be used for the direct synthesis of electrode materials. This approach of transformation at ambient temperature and pressure will open new areas for creating novel functional nanomaterials.

■ ASSOCIATED CONTENT

Supporting Information

The Supporting Information is available free of charge at <https://pubs.acs.org/doi/10.1021/acs.jpcc.1c00166>.

Large-area TEM and FESEM images of NDs and OLCs, TEM and FESEM images of OLCs from ES of 5 mM ND suspension, TEM images of the product obtained after ES on the ITO glass slide, schematic of SS setup, TEM images of OLCs obtained after ES using fused silica capillary, tabular comparison of Raman peaks of ND and OLC with the literature, calculation of the sp^2/sp^3 ratio, evaluation of the electric field, and Laplace pressure at the tip of the capillary (PDF)

■ AUTHOR INFORMATION

Corresponding Author

Thalappil Pradeep – DST Unit on Nanoscience, Thematic Unit of Excellence, Department of Chemistry, Indian Institute of Technology Madras, 600 036 Chennai, India; orcid.org/0000-0003-3174-534X; Phone: +91-044-2257-4208; Email: pradeep@iitm.ac.in

Authors

Deeksha Satyabola – DST Unit on Nanoscience, Thematic Unit of Excellence, Department of Chemistry, Indian Institute of Technology Madras, 600 036 Chennai, India

Tripti Ahuja – DST Unit on Nanoscience, Thematic Unit of Excellence, Department of Chemistry, Indian Institute of Technology Madras, 600 036 Chennai, India

Sandeep Bose – DST Unit on Nanoscience, Thematic Unit of Excellence, Department of Chemistry, Indian Institute of Technology Madras, 600 036 Chennai, India

Biswajit Mondal – DST Unit on Nanoscience, Thematic Unit of Excellence, Department of Chemistry, Indian Institute of Technology Madras, 600 036 Chennai, India

Pillalamarri Srikrishnarka – DST Unit on Nanoscience, Thematic Unit of Excellence, Department of Chemistry, Indian Institute of Technology Madras, 600 036 Chennai, India; orcid.org/0000-0001-5187-6879

M. P. Kannan – DST Unit on Nanoscience, Thematic Unit of Excellence, Department of Chemistry, Indian Institute of Technology Madras, 600 036 Chennai, India

B. K. Spoorthi – DST Unit on Nanoscience, Thematic Unit of Excellence, Department of Chemistry, Indian Institute of Technology Madras, 600 036 Chennai, India

Complete contact information is available at: <https://pubs.acs.org/doi/10.1021/acs.jpcc.1c00166>

Author Contributions

[†]Equal contribution. D.S. and T.A. contributed equally to this work. T.P., D.S., and T.A. conceived the idea and designed the experiments. D.S., T.A., and B.K.S. performed the experiments and analyzed the data. S.B. offered advice on the SS experiment. B.M., P.S., and M.P.K. performed imaging. The manuscript was written with the contribution of all authors. All authors have approved the final version of the manuscript.

Notes

The authors declare no competing financial interest.

■ ACKNOWLEDGMENTS

We thank the Department of Science and Technology (DST), Government of India, for constantly supporting our research

activities. D.S. acknowledges the Department of Chemistry, IIT Madras. T.A., S.B., B.M., and P.S. acknowledge the institute graduate fellowship. M.P.K. acknowledges MRF Ltd. B.K.S. acknowledges University Grants Commission (UGC) for her research fellowship.

■ REFERENCES

- (1) Shenderova, O. A.; Zhirnov, V. V.; Brenner, D. W. Carbon Nanostructures. *Crit. Rev. Solid State Mater. Sci.* **2002**, *27*, 227–356.
- (2) Georgakilas, V.; Perman, J. A.; Tucek, J.; Zboril, R. Broad Family of Carbon Nanoallotropes: Classification, Chemistry, and Applications of Fullerenes, Carbon Dots, Nanotubes, Graphene, Nanodiamonds, and Combined Superstructures. *Chem. Rev.* **2015**, *115*, 4744–4822.
- (3) Kroto, H. W.; Heath, J. R.; O'Brien, S. C.; Curl, R. F.; Smalley, R. E. C60: Buckminsterfullerene. *Nature* **1985**, *318*, 162–163.
- (4) Iijima, S. Helical Microtubules of Graphitic Carbon. *Nature* **1991**, *354*, 56–58.
- (5) Novoselov, K. S.; Geim, A. K.; Morozov, S. V.; Jiang, D.; Zhang, Y.; Dubonos, S. V.; Grigorieva, I. V.; Firsov, A. A. Electric Field Effect in Atomically Thin Carbon Films. *Science* **2004**, *306*, 666–669.
- (6) Ajayan, P. M. Nanotubes from Carbon. *Chem. Rev.* **1999**, *99*, 1787–1800.
- (7) Zeiger, M.; Jäckel, N.; Mochalin, V. N.; Presser, V. Review: Carbon Onions for Electrochemical Energy Storage. *J. Mater. Chem. A* **2016**, *4*, 3172–3196.
- (8) Mykhailiv, O.; Zubyk, H.; Plonska-Brzezinska, M. E. Carbon Nano-Onions: Unique Carbon Nanostructures with Fascinating Properties and Their Potential Applications. *Inorg. Chim. Acta* **2017**, *468*, 49–66.
- (9) Portet, C.; Yushin, G.; Gogotsi, Y. Electrochemical Performance of Carbon Onions, Nanodiamonds, Carbon Black and Multiwalled Nanotubes in Electrical Double Layer Capacitors. *Carbon* **2007**, *45*, 2511–2518.
- (10) Borgohain, R.; Li, J.; Selegue, J. P.; Cheng, Y.-T. Electrochemical Study of Functionalized Carbon Nano-Onions for High-Performance Supercapacitor Electrodes. *J. Phys. Chem. C* **2012**, *116*, 15068–15075.
- (11) Zheng, D.; Yang, G.; Zheng, Y.; Fan, P.; Ji, R.; Huang, J.; Zhang, W.; Yu, J. Carbon Nano-Onions as a Functional Dopant to Modify Hole Transporting Layers for Improving Stability and Performance of Planar Perovskite Solar Cells. *Electrochim. Acta* **2017**, *247*, 548–557.
- (12) Ghosh, M.; Sonkar, S. K.; Saxena, M.; Sarkar, S. Carbon Nano-Onions for Imaging the Life Cycle of *Drosophila Melanogaster*. *Small* **2011**, *7*, 3170–3177.
- (13) Sun, W.; Zhang, X.; Jia, H.-R.; Zhu, Y.-X.; Guo, Y.; Gao, G.; Li, Y.-H.; Wu, F.-G. Water-Dispersible Candle Soot-Derived Carbon Nano-Onion Clusters for Imaging-Guided Photothermal Cancer Therapy. *Small* **2019**, *15*, 1804575.
- (14) Trusel, M.; Baldrighi, M.; Marotta, R.; Gatto, F.; Pesce, M.; Frascini, M.; Catelani, T.; Papaleo, F.; Pompa, P. P.; Tonini, R.; et al. Internalization of Carbon Nano-Onions by Hippocampal Cells Preserves Neuronal Circuit Function and Recognition Memory. *ACS Appl. Mater. Interfaces* **2018**, *10*, 16952–16963.
- (15) Sohoul, E.; Shahdost-Fard, F.; Rahimi-Nasrabad, M.; Plonska-Brzezinska, M. E.; Ahmadi, F. Introducing a Novel Nanocomposite Consisting of Nitrogen-Doped Carbon Nano-Onions and Gold Nanoparticles for the Electrochemical Sensor to Measure Acetaminophen. *J. Electroanal. Chem.* **2020**, *871*, 114309.
- (16) Shao, H.; Zhang, X.; Huang, H.; Zhang, K.; Wang, M.; Zhang, C.; Yang, Y.; Wen, M.; Zheng, W. Magnetron Sputtering Deposition Cu@Onion-like N-C as High-Performance Electrocatalysts for Oxygen Reduction Reaction. *ACS Appl. Mater. Interfaces* **2017**, *9*, 41945–41954.
- (17) Porada, S.; Borchardt, L.; Oschatz, M.; Bryjak, M.; Atchison, J. S.; Keesman, K. J.; Kaskel, S.; Biesheuvel, P. M.; Presser, V. Direct Prediction of the Desalination Performance of Porous Carbon

Electrodes for Capacitive Deionization. *Energy Environ. Sci.* **2013**, *6*, 3700–3712.

(18) de Heer, W. A.; Ugarte, D. Carbon Onions Produced by Heat Treatment of Carbon Soot and Their Relation to the 217.5 Nm Interstellar Absorption Feature. *Chem. Phys. Lett.* **1993**, *207*, 480–486.

(19) Ugarte, D. Curling and Closure of Graphitic Networks under Electron-Beam Irradiation. *Nature* **1992**, *359*, 707–709.

(20) Kuznetsov, V. L.; Chuvilin, A. L.; Butenko, Y. V.; Mal'kov, I. Y.; Titov, V. M. Onion-like Carbon from Ultra-Disperse Diamond. *Chem. Phys. Lett.* **1994**, *222*, 343–348.

(21) Tomita, S.; Sakurai, T.; Ohta, H.; Fujii, M.; Hayashi, S. Structure and Electronic Properties of Carbon Onions. *J. Chem. Phys.* **2001**, *114*, 7477–7482.

(22) Chen, X. H.; Deng, F. M.; Wang, J. X.; Yang, H. S.; Wu, G. T.; Zhang, X. B.; Peng, J. C.; Li, W. Z. New Method of Carbon Onion Growth by Radio-Frequency Plasma-Enhanced Chemical Vapor Deposition. *Chem. Phys. Lett.* **2001**, *336*, 201–204.

(23) Cabioch, T.; Jaouen, M.; Thune, E.; Guérin, P.; Fayoux, C.; Denanot, M. F. Carbon Onions Formation by High-Dose Carbon Ion Implantation into Copper and Silver. *Surf. Coating Technol.* **2000**, *128–129*, 43–50.

(24) Alexandrou, I.; Wang, H.; Sano, N.; Amaratunga, G. A. J. Structure of Carbon Onions and Nanotubes Formed by Arc in Liquids. *J. Chem. Phys.* **2004**, *120*, 1055–1058.

(25) Garcia-Martin, T.; Rincon-Arevalo, P.; Campos-Martin, G. Method to Obtain Carbon Nano-Onions by Pyrolysis of Propane. *Cent. Eur. J. Phys.* **2013**, *11*, 1548–1558.

(26) Choucair, M.; Stride, J. A. The Gram-Scale Synthesis of Carbon Onions. *Carbon* **2012**, *50*, 1109–1115.

(27) Gubarevich, A. V.; Kitamura, J.; Usuba, S.; Yokoi, H.; Kakudate, Y.; Odawara, O. Onion-like Carbon Deposition by Plasma Spraying of Nanodiamonds. *Carbon* **2003**, *41*, 2601–2606.

(28) Xiao, J.; Li, J. L.; Liu, P.; Yang, G. W. A New Phase Transformation Path from Nanodiamond to New-Diamond via an Intermediate Carbon Onion. *Nanoscale* **2014**, *6*, 15098–15106.

(29) Banerjee, S.; Mazumdar, S. Electrospray Ionization Mass Spectrometry: A Technique to Access the Information beyond the Molecular Weight of the Analyte. *Int. J. Anal. Chem.* **2012**, *2012*, 1–40.

(30) Li, A.; Luo, Q.; Park, S.-J.; Cooks, R. G. Synthesis and Catalytic Reactions of Nanoparticles Formed by Electrospray Ionization of Coinage Metals. *Angew. Chem., Int. Ed.* **2014**, *53*, 3147–3150.

(31) Sarkar, D.; Mahitha, M. K.; Som, A.; Li, A.; Wlekinski, M.; Cooks, R. G.; Pradeep, T. Metallic Nanobrushes Made Using Ambient Droplet Sprays. *Adv. Mater.* **2016**, *28*, 2223–2228.

(32) Jana, A.; Jana, S. K.; Sarkar, D.; Ahuja, T.; Basuri, P.; Mondal, B.; Bose, S.; Ghosh, J.; Pradeep, T. Electrospray Deposition-Induced Ambient Phase Transition in Copper Sulphide Nanostructures. *J. Mater. Chem. A* **2019**, *7*, 6387–6394.

(33) Kebarle, P.; Tang, L. From Ions in Solution to Ions in the Gas Phase - the Mechanism of Electrospray Mass Spectrometry. *Anal. Chem.* **1993**, *65*, 972A–986A.

(34) Chowdhury, S. K.; Chait, B. T. Method for the Electrospray Ionization of Highly Conductive Aqueous Solutions. *Anal. Chem.* **1991**, *63*, 1660–1664.

(35) Karas, M.; Bahr, U.; Dülcks, T. Nano-Electrospray Ionization Mass Spectrometry: Addressing Analytical Problems beyond Routine. *Fresenius. J. Anal. Chem.* **2000**, *366*, 669–676.

(36) Iavarone, A. T.; Jurchen, J. C.; Williams, E. R. Effects of Solvent on the Maximum Charge State and Charge State Distribution of Protein Ions Produced by Electrospray Ionization. *J. Am. Soc. Mass Spectrom.* **2000**, *11*, 976–985.

(37) Inel, G. A.; Ungureau, E.-M.; Varley, T. S.; Hirani, M.; Holt, K. B. Solvent-Surface Interactions between Nanodiamond and Ethanol Studied with in Situ Infrared Spectroscopy. *Diam. Relat. Mater.* **2016**, *61*, 7–13.

(38) Nunn, N.; Torelli, M.; McGuire, G.; Shenderova, O. Nanodiamond: A High Impact Nanomaterial. *Curr. Opin. Solid State Mater. Sci.* **2017**, *21*, 1–9.

(39) Pentecost, A.; Gour, S.; Mochalin, V.; Knoke, I.; Gogotsi, Y. Deaggregation of Nanodiamond Powders Using Salt- and Sugar-Assisted Milling. *ACS Appl. Mater. Interfaces* **2010**, *2*, 3289–3294.

(40) Israde-Alcántara, I.; Bischoff, J. L.; Domínguez-Vázquez, G.; Li, H. C.; DeCarli, P. S.; Bunch, T. E.; Wittke, J. H.; Weaver, J. C.; Firestone, R. B.; West, A.; et al. Evidence from Central Mexico Supporting the Younger Dryas Extraterrestrial Impact Hypothesis. *Proc. Natl. Acad. Sci. U. S. A.* **2012**, *109*, E738–E747.

(41) Mermoux, M.; Crisci, A.; Petit, T.; Girard, H. A.; Arnault, J.-C. Surface Modifications of Detonation Nanodiamonds Probed by Multiwavelength Raman Spectroscopy. *J. Phys. Chem. C* **2014**, *118*, 23415–23425.

(42) Mermoux, M.; Chang, S.; Girard, H. A.; Arnault, J.-C. Raman Spectroscopy Study of Detonation Nanodiamond. *Diam. Relat. Mater.* **2018**, *87*, 248–260.

(43) Cebik, J.; McDonough, J. K.; Peerally, F.; Medrano, R.; Neitzel, I.; Gogotsi, Y.; Osswald, S. Raman Spectroscopy Study of the Nanodiamond-to-Carbon Onion Transformation. *Nanotechnology* **2013**, *24*, 205703.

(44) Mykhaylyk, O. O.; Solonin, Y. M.; Batchelder, D. N.; Brydson, R. Transformation of Nanodiamond into Carbon Onions: A Comparative Study by High-Resolution Transmission Electron Microscopy, Electron Energy-Loss Spectroscopy, X-Ray Diffraction, Small-Angle x-Ray Scattering, and Ultraviolet Raman Spectroscopy. *J. Appl. Phys.* **2005**, *97*, 074302.

(45) Xie, F. Y.; Xie, W. G.; Gong, L.; Zhang, W. H.; Chen, S. H.; Zhang, Q. Z.; Chen, J. Surface Characterization on Graphitization of Nanodiamond Powder Annealed in Nitrogen Ambient. *Surf. Interface Anal.* **2010**, *42*, 1514–1518.

(46) Lee, J. K.; Samanta, D.; Nam, H. G.; Zare, R. N. Spontaneous Formation of Gold Nanostructures in Aqueous Microdroplets. *Nat. Commun.* **2018**, *9*, 1562.

(47) Kim, H.-H.; Kim, J.-H.; Ogata, A. Time-Resolved High-Speed Camera Observation of Electrospray. *J. Aerosol Sci.* **2011**, *42*, 249–263.

(48) Lee, S.; Kim, D. H.; Needham, D. Equilibrium and Dynamic Interfacial Tension Measurements at Microscopic Interfaces Using a Micropipet Technique. I. A New Method for Determination of Interfacial Tension. *Langmuir* **2001**, *17*, 5537–5543.

(49) Siders, C. W.; Cavalleri, A.; Sokolowski-Tinten, K.; Tóth, C.; Guo, T.; Kammler, M.; von Hoegen, M. H.; Wilson, K. R.; von der Linde, D.; Barty, C. P. J. Detection of Nonthermal Melting by Ultrafast X-Ray Diffraction. *Science* **1999**, *286*, 1340–1342.

(50) Rousse, A.; Rischel, C.; Fourmaux, S.; Uschmann, I.; Sebban, S.; Grillon, G.; Balcou, P.; Förster, E.; Geindre, J. P.; Audebert, P.; et al. Non-Thermal Melting in Semiconductors Measured at Femtosecond Resolution. *Nature* **2001**, *410*, 65–68.

(51) Iglev, H.; Schmeisser, M.; Simeonidis, K.; Thaller, A.; Laubereau, A. Ultrafast Superheating and Melting of Bulk Ice. *Nature* **2006**, *439*, 183–186.

(52) Schäfer, H. Introduction and Historical Review. *Chem. Transp. React.* **1964**, *3*, 1–3.

(53) Banerjee, S.; Zare, R. N. Syntheses of Isoquinoline and Substituted Quinolines in Charged Microdroplets. *Angew. Chem.* **2015**, *127*, 15008–15012.